Mechanical characterization of additively manufactured photopolymerized polymers

Roberto Brighenti, Liviu Marsavina, Mihai P. Marghitas, Mattia P. Cosma & Matteo Montanari

Published online: 11 Mar 2022.

Submit your article to this journal ⬈

View related articles ⬈

View Crossmark data ⬈

ORIGINAL ARTICLE

Mechanical characterization of additively manufactured photopolymerized polymers

Roberto Brighenti[a], Liviu Marsavina[b] , Mihai P. Marghitas[b], Mattia P. Cosma[a], and Matteo Montanari[a]

[a]Department of Engineering and Architecture, University of Parma, Parma, Italy; [b]Department of Mechanics and Strength of Materials, University Politehnica Timisoara, Timisoara, Romania

ABSTRACT

Photopolymerization, based on light-induced radical polymerization, is nowadays exploited in additive manufacturing (AM) technologies enabling to achieve high dimensional quality. The mechanical properties of the obtained material are heavily dependent on the chemistry of the photopolymer and on the way the AM process is performed. Here we study, through experiments and theoretical modeling, how the mechanical properties of liquid crystal shutter (LCD) printed photopolymers depend on the printing process setup, namely UV exposure time and layer thickness. To this end, a multi-physics simulation tool considering the light diffusion, chemical kinetics, and the micro-mechanics at the network level, has been developed.

Nomenclature

A	Attenuation coefficient or absorbance
b	Length of Kuhn's segments
C_I	Concentration of photo-initiator molecules (Φ)
C_M	Concentration of monomer molecules (M)
C_R	Concentration of free radicals ($R^\bullet$)
c_a	Concentration of active chains
E	Young's modulus
$\boldsymbol{f}(\boldsymbol{r})$	Force in a single polymer chain
$\boldsymbol{F}$	Deformation gradient
h, h_i	Specimen's thickness and layer thickness, respectively
I	Laser light intensity
I_0	Maximum laser light intensity on the irradiated surface
$J = \det \boldsymbol{F}$	Volume change ratio of the material
k_B	Boltzmann's constant
k_p, k_t	Reaction rate constants
$\boldsymbol{l}(\boldsymbol{X}, t)$	Unit vector identifying the incoming light beam
$\mathcal{L}$, $\mathcal{L}^{-1}$	Langevin function and its inverse, respectively
$\boldsymbol{L}$	Velocity of deformation tensor
N	Number of Kuhn's segments per chain
$\boldsymbol{n}$	Unit vector normal to the free surface of the domain hit by the beam light
m	Number of radicals generated in the photodecomposition
$\boldsymbol{P}$	First Piola stress tensor
$P^\bullet$	Functional groups (growing polymer chains)
P_{dead}	Dead polymer chains (grown polymer chains)
$R^\bullet$	Free radicals
t	Time
t_c	Curing time
T	Absolute temperature
β	Function approximating the inverse Langevin function $\mathcal{L}^{-1}$
$\varphi(\boldsymbol{r})$, $\varphi_0(\boldsymbol{r})$	Dimensionless distribution function of the chains' end-to-vector and the corresponding one at the initial stress-free state, respectively
γ	Photodecomposition rate
$\mu, \overline{\mu}$	Shear modulus and shear modulus of the fully-cured material, respectively
$\psi(\boldsymbol{r})$	Deformation energy of a single polymer chain
Ψ	Energy per unit volume of a deformed polymer
$\rho(\boldsymbol{r})$	Distribution function of the chains' end-to-end vector
ϱ	Degree of cure (or degree of conversion, DoC) achieved during the photopolymerization
$\boldsymbol{\sigma}$	Cauchy stress
$[\blacksquare]$	Concentration of the chemical species represented by $\blacksquare$

1. Introduction

In the last decades, a tremendous development of Additive Manufacturing (AM) technologies has revolutionized the way objects are produced in industry, allowing to create elements spanning an extremely large scale range with unprecedented precision, not achievable by traditional production procedures [1–4].

Differently from traditional production methods – typically based on material subtraction processing, cast or molding – AM technologies operate by adding layer-by-layer (such as in the fusion deposition modeling, FDM, and the digital light processing, DLP, among others) or small volume-by-small volume (such as in the selective laser sintering, SLS, and the stereolitography, SLA, among others) to obtain the final part. The endless production possibilities offered by AM and the variety of printable materials (from metals to ceramics, plastics and even biological matters) enable its use in a wide spectrum of application fields, ranging from daily life products [5], automotive [6], aerospace [7], printed electronics [8], healthcare and biomedicine [9], smart and responsive materials [10], architected materials

[11], composite materials [12], highly-deformable elastomers [13], to mention a few.

Among the AM technologies developed so far, those devoted to print polymers have had an impressive advancement in the last years; in particular, those based on the solidification of an initial liquid monomer resin through a light-induced polymerization reaction, enable the production of elements at very different length scales, characterized by a very high resolution (layer thicknesses down to 20-25 μm can be obtained nowadays) [14].

Photopolymerization is based on a chemical-physical process which, starting from a liquid monomer solution, leads to a three-dimensional solid polymeric material whose solidification occurs by spreading light of a suitable wavelength (typically UV light, whose wavelength falls within the range 300-400 nm), in a spatially controlled way according to the component's digital model [15]. The photopolymerization chemical-physical process is used in the Stereolithography (SLA) technology, where the liquid monomer resin is irradiated by a moving light beam inducing the polymerization and thus the solidification of adjacent portions of the material [16]. More recently, photopolymerization has been implemented in the so-called Digital Light Processing (DLP) technology, which operates by directly projecting the UV-light over the whole cross-section of the object being printed, leading to the solidification of an entire layer in a single shot. The photopolymerization process has been also exploited in the so-called Continuous Liquid Interface Production (CLIP), which employs a bottom-up printing procedure allowing to achieve continuous printing by creating a permeable window aimed at decreasing the detrimental effects of oxygen inhibition on the polymerization reaction [17].

Structures and components characterized by a multi-material topology can be easily obtained with additive manufacturing; this is well-known and trivial for AM technologies based on material extrusion such as FDM, but nowadays it can be achieved also within the photopolymerization 3 D printing approach (by using SLA, DLP and CLIP), for instance by manually/mechanically switching resin or by adopting other approaches [18].

The everyday use of AM production techniques, especially those based on complex chemical-physical processes, require special care if reliable mechanical properties are sought; in fact, the performance of printed parts is a complex combination of the raw material and of the setting of the AM procedure adopted during the printing process. This implies that, even starting with the same raw material, geometrically identical printed elements can have different mechanical performances according to the way the AM process is performed [19].

The achievement of well-defined and reliable mechanical properties of AM parts requires the 3 D printing process to be carefully understood and modeled, by properly quantitatively describing the physics and chemistry of the involved phenomena. This can be achieved through suitable mathematical models; their implementation in a computational framework becomes unavoidable when the complexity of the domain and the boundary conditions of the problem being studied do not allow an analytical solution. This problem has been quite often tackled by adopting a trial and error experimental-based iterative approach, where the effects of different AM setups are quantified through test measurements performed on the corresponding printed parts [20]. This approach, beyond being time consuming, cannot be straightforwardly extended to other cases in which different scenarios and/or (slightly) different AM procedures are employed.

A precise mathematical description of the chemical-physical phenomena involved in the AM process, whose applicability and generality can be easily appreciated, represents a soundness and scientifically-based alternative to empirical approaches [21–23]. In photopolymerization-based AM technologies, the main foundation of the theoretical approach is represented by the mathematical description of the kinetics of the process, typically formulated through a set of partial differential equations providing the evolution of the concentration of reactant variables involved in the curing process [24]. Moreover, once the liquid-solid conversion during printing has been quantified, the characteristics of the obtained polymer's network have to be related – for instance by using the well-known rubber elasticity theory [25] – to the macroscopic mechanical properties of the final material [26].

In the present study, we consider how the time exposure to the UV source light triggering the photopolymerization and the thickness of the printed layers (which are often the main AM parameters to be set) are relevant to the final material properties. It is shown through experimental tests that slightly different choices of the above-mentioned parameters can lead to quite different mechanical properties of the final polymer. In particular, it is considered how the Young's modulus and the tensile strength (the most useful mechanical parameters in real applications) can be tuned by properly driving the photopolymerization process.

Further, we consider the theoretical description of the chemical-physical phenomena taking place during photopolymerization, in order to quantitatively evaluate the main mechanical characteristics of the obtained printed parts. This multi-physics approach can be conveniently exploited, for instance, in both the SLA and DLP AM technologies. To this end, we first consider the light diffusion process within the liquid resin bath and, according to the point wise time history of the light intensity, the monomer-polymer chain conversion [27] and its relation to the mechanical characteristics of the final material.

Therefore, the whole theoretical model requires three phases, which can be modeled and solved in a staggered way, by considering: i) the generalized Beer-Lambert law providing the light diffusion in a semi-transparent material, ii) the kinetics of the light-driven radical polymerization reactions and iii) a physics-based approach, hereafter assumed to be rooted in the network's chain statistics micromechanical model, enabling to link the polymer's degree of cure (DoC) produced by the photopolymerization process to the mechanical characteristics. This multi-physics approach allows us to control all the liquid-solid transition phases, and can be usefully adopted to design and optimize the AM
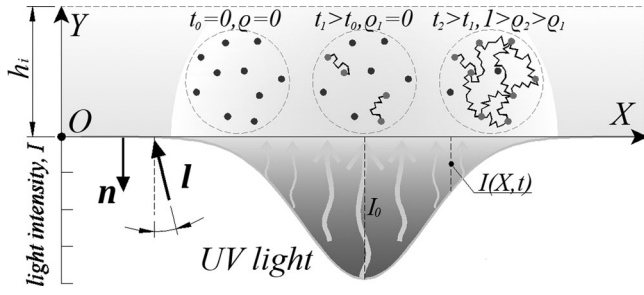
Figure 1. Scheme of the photopolymerization reaction: initially, the photo-initiators contained in the liquid monomer resin are inactive (t_0). By UV light irradiation, the photo-initiators convert into free radicals which react with the monomer molecules triggering the growth of the polymer chains. The amount of created chains is quantified by the degree of cure $\varrho = \varrho(t)$.

procedure according to the final properties required by the printed object. It is shown that such an approach represents a suitable and precise tool to evaluate the macroscopic mechanical features of additively manufactured parts, allowing the AM process to be accurately designed and controlled in order to obtain the best mechanical performances according to the specific application of interest.

The paper is organized as follows: Section 2 illustrates the phenomena involved in the photopolymerization process and their mathematical description. Section 3 presents the physics-based mechanical model of the polymer network, aimed at linking the polymer chain network characteristics to the elasticity and strength properties of the printed material. Section 4 illustrates the experimental mechanical tests conducted on specimens obtained through different settings of the AM process, while Section 5 presents some applications of the proposed model aimed at demonstrating its reliability in assessing the mechanical characteristics of the printed material. Finally, Section 6 outlines some conclusions and describes future research directions in the topic.

2. Photopolymerization governing equations

The photopolymerization process encompasses different chemical-physical phenomena, whose quantitative description and reciprocal interaction are required to correctly assess the characteristics of the obtained material. In the following, starting from the light diffusion up to the mechanics of the photopolymerized material, the governing equations describing the process are illustrated in detail.

2.1. Light diffusion

The first physical phenomenon to be quantified is the light diffusion within a semi-transparent medium. Typically, a UV light source – which can be at rest (such as in the DLP) or moving with a given speed (such as in the SLA) – is used to induce the photopolymerization. The light beam hits the surface of the liquid bath and spreads inside the fluid matter where it is attenuated while going in depth in the medium. The kinetics of the photopolymerization process (see Section 2.2) requires the point wise intensity of the light to be known. The Beer-Lambert law, which requires the knowledge in time of the material absorbance distribution within

the domain, is usually adopted to describe such a phenomenon [28].

Let us consider the 3D domain Ω_0, having boundary $\partial\Omega_0$, to be involved in the light diffusion process; by adopting a cartesian coordinate frame of reference whose points are identified by the position vector $\mathbf{X}$ in the initial (undeformed) configuration, the light diffusion equation and its boundary conditions (B.Cs) read:

$$\mathbf{l}(\mathbf{X}, \ t) \cdot \nabla_{\mathbf{X}} I(\mathbf{X}, \ t) = -A(\mathbf{X}, \ t) \ I(\mathbf{X}, \ t) \text{ for } \mathbf{X} \in \Omega_0 \quad (1a)$$

$$I(\mathbf{X}, \ t) = I_0(\mathbf{X}, \ t) \text{ for } \mathbf{X} \in \partial\Omega_0 \quad (1b)$$

where $I(\mathbf{X}, \ t)$ is the light intensity at the position $\mathbf{X} = (X, Y, Z)$ and time t, $\mathbf{l}(\mathbf{X}, \ t)$ is the unit vector of the incoming light beam, $\nabla_{\mathbf{X}}$ indicates the gradient operator and $A(\mathbf{X}, \ t)$ is the absorbance (i.e. the light attenuation coefficient) quantifying the light intensity reduction (due to photons that are stopped in their motion because of scattering and/or absorption) while going in depth in the material. In a one-dimensional case where the light travels along the Y-direction only and the absorbance is assumed to be constant, the solution of the above equation is given by: $I(Y, \ t) = I_0(t)\exp(-AY)$ where the exponential attenuation of the light intensity by increasing the depth Y can be appreciated.

In a generic setting, the problem (1a)-(1b) needs to be solved numerically, for instance by implementing the governing equations and the related B.Cs into a finite element (FE) framework. Further, it has to be considered that the light attenuation coefficient $A(\mathbf{X}, \ t)$ usually has a complex dependence on the concentration of the chemical species present in the medium, such as those of photo-initiators, photo-absorbers, monomers and polymerized monomers [24]. Due to the dependence of $A(\mathbf{X}, \ t)$ on quantities whose evolution is a function of the light intensity field, the problem results to be highly non-linear.

2.2. Kinetics of chemical species evolution during photopolymerization

The light radiation going inside the material is absorbed by photo-initiators, photo-absorbers, and by other light reactive species present in the matrix, leading to a liquid (monomers) → solid (polymer chains) transformation. Such a solidification process takes place thanks to the following phenomena: the light radiation induces the photo-initiators molecules Ph_I, whose concentration in the liquid monomer bath is $C_I(X,t)$, to be converted into free radicals $R^\bullet$ ($Ph_I \overset{\gamma}{\rightarrow} 2R^\bullet$) whose concentration is $C_R(X,t)$. Then, free radicals react with monomer molecules (M) inducing the appearance of functional groups $P^\bullet$ ($R^\bullet + M \rightarrow P^\bullet$), which constitute growing chains whose evolution in space (chain growth: $P^\bullet + M \overset{k_p}{\rightarrow} P^\bullet$) is interrupted either when the polymer chain encounters a free radical (in symbols: $P^\bullet + R^\bullet \overset{k_t}{\rightarrow} P_{dead}$) or when it joints to another chain encountered along its growing path ($P^\bullet + P^\bullet \overset{k_t}{\rightarrow} P_{dead}$) [22]. In the above relations γ, k_p and k_t are reaction rate parameters, depending on the environmental conditions, such as the temperature,
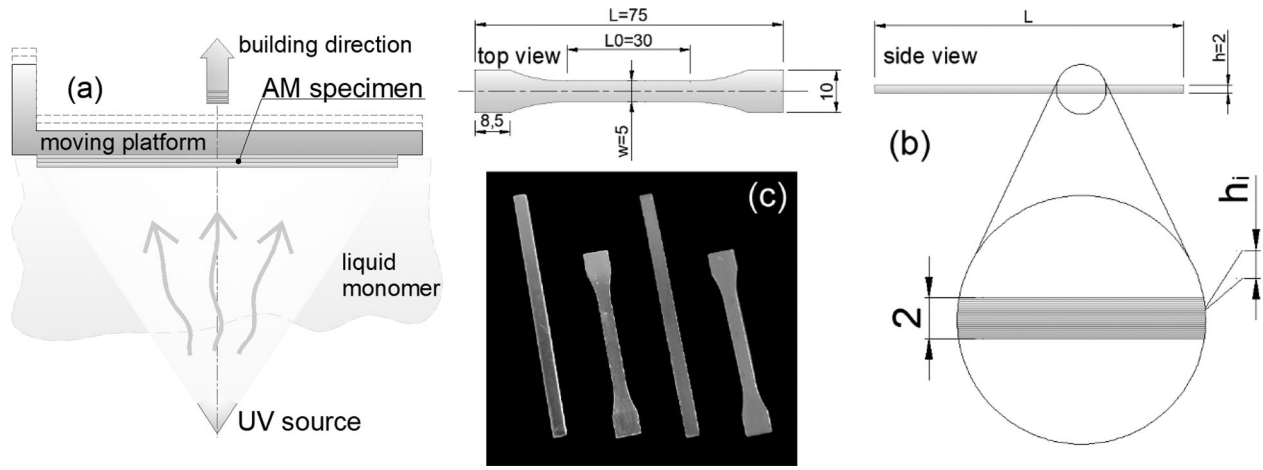
Figure 2. Scheme of the DLP AM process used to print the specimens to be mechanically tested (a). Sizes of the printed specimens (in mm) and detail of their layered structure (each specimen has all the layers with the same thickness h_i) (b). Images of the smooth and dog bone printed specimens for the two considered photoresins (c).

characterizing the chemical process. For the sake of simplicity, in the following all the involved chemical processes are assumed to be isothermal so the above rates are constant. The above-described photopolymerization kinetics is representative of a conventional radical polymerization, which is the polymerization mechanism considered in the present study. It is worth mentioning that, in contrast to conventional radical polymerization, the so-called reversible deactivation radical polymerization (RDRP) exists. This latter chemical-physical transformation, whose kinetic mechanism is governed by the same laws of the conventional radical polymerization, allows obtaining a polymer characterized by a "living" or "controlled" radical polymerization. RDRP typically exploits the ability of some chemical species inserted in the resin being printed, of reversibly controlling the propagation of radical species (and thus of polymer chains), allowing for a precise tuning of the polymer chains architecture. This makes possible to obtain intriguing post-synthesis transformations level such as self-healing, network alterations, etc., taking place at the molecular level [29, 30].

The photo-induced polymerization progressively reduces the monomer concentration in the liquid bath and makes the polymer chains to appear; the amount of monomer → polymer conversion is typically quantified by the so-called degree of cure [24]:

$$\varrho(\mathbf{X}, t) = 1 - C_M(\mathbf{X}, t) \ C_{M_0}^{-1} \qquad (2)$$

where $C_{M_0} = C_M(\mathbf{X}, t = 0)$ is the initial concentration of the monomer molecules in the liquid resin. Such a parameter starts from zero when the solidification has not yet started, and tends to one when all the monomers molecules have been converted into polymer chains (Figure 1).

The scalar parameter ϱ can be related to the concentration of chains $c_a(\mathbf{x}, t)$ (number of chains per unit volume) formed inside the initially liquid domain; in particular, we are interested in quantifying the chains composing the load bearing network of the polymer; from our viewpoint, the chain concentration quantifies only the active chains, i.e. those fully connected to the polymer network. The $c_a - \varrho$ relationship can be expressed through the exponential function [31]:

$$c_a(\mathbf{X}, t) = \frac{\mu(\mathbf{X}, t)}{k_B T}$$
$$= \begin{cases} \dfrac{1}{3 \ k_B T} \{E_d + E_c \exp[s(\varrho(\mathbf{X}, t) - \varrho_{gel})]\} & \text{if } \varrho(\mathbf{X}, t) > \varrho_{gel} \\ 0 & \text{if } \varrho(\mathbf{X}, t) \le \varrho_{gel} \end{cases}$$
$$(3)$$

where the well-known rubber-elasticity relationship $\mu = c_a k_B T$, linking the shear modulus μ to the chain concentration c_a, has been introduced; in Eq. (3) k_B, T are the Boltzmann constant and the absolute temperature, respectively, ϱ_{gel} is the degree of cure corresponding to the monomer liquid starting to become solid, and E_c, E_d, s are fitting parameters.

By assuming $\varrho_{gel} \cong 0$ and by indicating with $\overline{\mu} = k_B T \ \overline{c}_a = k_B T \ c_a(\mathbf{X}, t \to \infty)$ the shear modulus of the fully cured polymer (corresponding to the maximum chain concentration $\overline{c}_a$ achievable by exposing the monomer material to light for an unlimited time and neglecting any degradation phenomena), the chain concentration-degree of cure relationship (3) can be alternatively expressed as:

$$c_a(\mathbf{X}, t) = \underbrace{\left(\frac{\overline{\mu}}{k_B T}\right)}_{\overline{c}_a} \cdot \exp[\alpha(\varrho(\mathbf{X}, t) - 1)] \qquad (4)$$

where $c_{a0} = \frac{\overline{\mu}}{k_B T} \exp(-\alpha)$ is the active chain concentration (usually small) present in the material in its initial (nearly) liquid state. According to Eq. (A4), the time rate of the degree of cure $\dot{\varrho}(\mathrm{X}, t)$ tends to zero as the monomer concentration C_M vanishes being consumed in building the chain network. Consequently, $\varrho(\mathbf{X}, t \to \infty) \to 1$ and $c_a(\mathbf{X}, t \to \infty) \to \overline{c}_a$, see Eq. (4). More details on the chemical kinetics governing equations are provided in Appendix A.

The chain concentration rate can be finally evaluated as $\dot{c}_a(\mathbf{X}, t) = \alpha \ \overline{c}_a \ \dot{\varrho}(\mathbf{X}, t)$ and used to assess the current chain concentration by time integration, i.e. $c_a(\mathbf{X}, t_c) = c_{a0}(\mathbf{X}) + \int_0^{t_c} \dot{c}_a(\mathbf{X}, t) \ dt$, where the time interval $0 \div t_c$ represents the curing time.
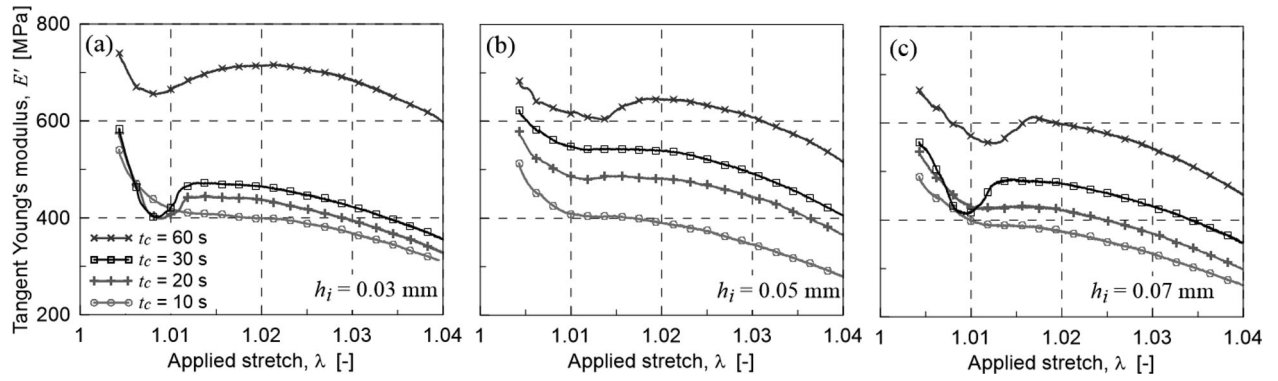
Figure 3. Photopolymer No. 1. Tangent Young's modulus vs applied stretch for different exposure times ($t_c = 10, 20, 30, 60 \, s$) and layer thicknesses adopted in the photopolymerization process: $h_i = 0.03 \, mm$ (a), $h_i = 0.05 \, mm$ (b), $h_i = 0.07 \, mm$ (c).

3. Experimental tests

The influence of the main photopolymerization parameters on the mechanical characteristics of AM printed parts is here investigated. Several specimens, printed by using two different photopolymers and varying the curing exposure time and the layer thickness, have been mechanically tested in order to determine the tensile strength and the elastic modulus. In particular, a 3D LCD printer (Anycubic Photon® and Anycubic wash and post cure machine 2.0®) has been used to prepare the specimens.

LCD 3D printing operates nearly as DLP technology; it is based on flashing complete layers at the resin tank with the UV light coming from an array of LEDs shining through a liquid crystal shutter (LCD), while a projector is usually adopted in the DLP technology. The screen operates as a mask allowing the light to shine only the regions to be printed for the current layer, and no special device is required to direct light as occurs for SLA- or DLP-based printers.

The printed specimens have been prepared according to the following parameters: the light exposure time has been assumed to be equal to $t_c = 10, 20, 30$ and $60 s$ for each layer (for the photopolymer No. 1, Anycubic® UV sensitive resin, "*translucent green*", curing UV light wavelength 405 nm) and $t_c = 15, 20, 30$ and $60 s$ (for the photopolymer No. 2, Anycubic® UV sensitive resin, "*clear*", UV curing light wavelength 405 nm), and the thickness of the layers composing the part to be printed have been made to assume the following values: $h_i = 0.03, 0.05, 0.07 \, mm$) (Figure 2). The geometry of the AM specimens and the testing procedure (determination of the tensile properties of plastics) has been assumed in accordance with the ISO 527-1 code [32]. It is worth mentioning that for the photopolymer No. 2 the minimum curing time has been assumed equal to 15 s because the time exposure $t_c = 10 \, s$ was too short to solidify the initial liquid photoresin. Four specimens have been tested for each photopolymerization setting.

Both static tensile and cyclic tests have been performed: per each printing condition (exposure time and layer thickness) 4 smooth and 4 dog bone specimens have been tested under static tension per each photopolymer type. Cyclic tests have been performed on different smooth specimens per each maximum cycle's deformation and per each photoresin by adopting the exposure time $t_c = 30s$ and $h_i = 0.03 \, mm$.

Static tensile tests have been performed (a universal testing machine Galdabini® Quasar 2.5 has been used), by adopting a displacement rate equal to $\dot{\delta} = 5 \, mm/min$, corresponding to a stretch rate $\dot{\lambda} \cong 0.018 \, s^{-1}$. The tensile strength and the tangent elastic modulus *vs* the applied deformation have been determined for all the photopolymerization setups defined above. As already mentioned, two different photoresins, characterized by a different absorbivity value, resin No. 1 ($A = 304 \, m^{-1}$) and resin No. 2 ($A = 147 \, m^{-1}$), have been used. For each material, the absorbivity has been evaluated by using printed plates of different thickness ($h = 3 \div 6 \, mm$), obtained by adopting different exposure times ($10 \div 60 \, s$ for the photopolymer No. 1 and $15 \div 60 \, s$ for the photopolymer No. 2). The absorbance has been calculated by using the solution of the one dimensional light diffusion equation (see Sect. 2.1) through the expression $A = \frac{ln(I_a) - ln(I)}{h}$; the light intensities measured above (I_a) and below (I) the irradiated flat plate exposed to a uniform light source from the top, have been measured for such a purpose. The obtained values are almost independent of the photopolymerization exposure time, indicating that the degree of solidification of the polymer does not alter significantly the transparency and thus the absorbance of the material. Finally, the curing light intensity provided by the DLP printer (wavelength 405 nm) has been measured to be equal to $I_0(t) = 7.321 \cdot 10^{-4} \, mW/cm^2, \, \forall t$.

The experimental outcomes are represented by the tangent Young's modulus, determined within the whole deformation range spanned by the mechanical tests until failure, and the tensile strength; in the following figures, the obtained results are displayed for the two photopolymers analyzed.

Figure 3 clearly shows that the tangent Young's modulus decreases by decreasing the exposure time and by increasing the layer thickness; printing with a thinner layer ensures a slightly greater material's elastic modulus. By considering the experimental results related to the elastic modulus when the curing time t_c increases, it is possible to extrapolate the shear modulus of the fully cured photopolymer No. 1 which turns out to be equal to about $\bar{\mu} = 210 \, MPa$. Figure 4, which displays the experimentally determined average values and the related standard deviations of the strength (Figure 4a) and of the elastic modulus (Figure 4b), summarizes the mechanical test results for the photopolymer No. 1. The theoretical model illustrated in Section 2 (parameters of the model: $k_p = k_t = 0.6 \, \frac{m^3}{mol \cdot s}, \quad \gamma = 8 \cdot 10^{-3} \frac{s^2}{kg}, \quad \alpha = 3, \quad C_I = 1000 \frac{mol}{m^3}, \, C_{M0} = 3000 \frac{mol}{m^3}, \, C_R = 0 \frac{mol}{m^3}, \, A = 304 \, m^{-1}$) has been used to assess the elastic modulus of the photopolymerized polymer and the
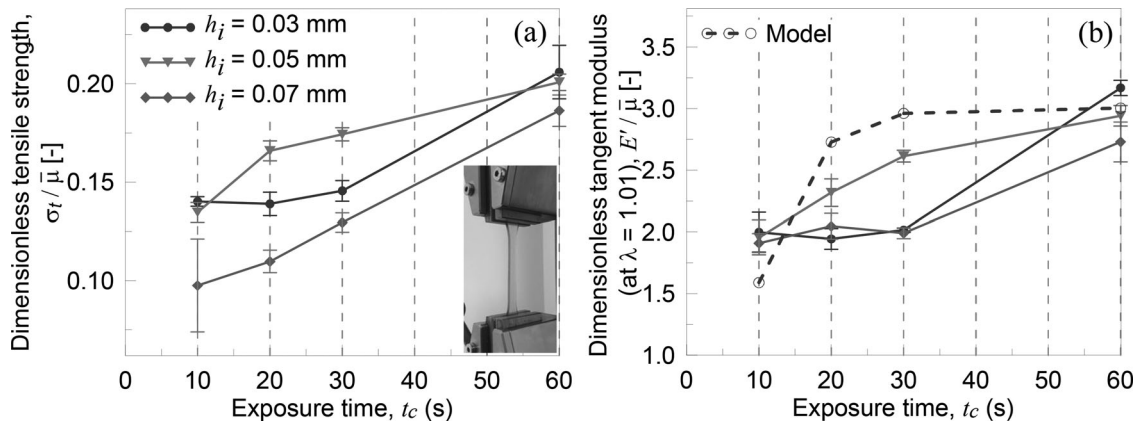
Figure 4. Photopolymer No. 1. Dimensionless mean tensile strength and dimensionless mean tangent Young's modulus (determined at the deformation $\lambda = 1.01$) vs exposure time for different layer thicknesses ($h_i = 0.03,\ 0.05,\ 0.07\ mm$).
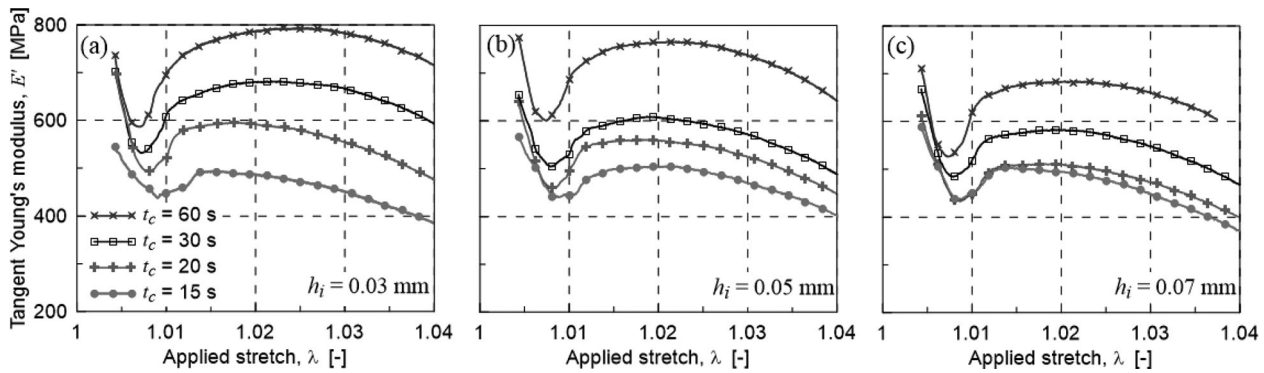

Figure 5. Photopolymer No. 2. Tangent Young's modulus vs applied stretch for different exposure times ($t_c = 10,\ 20,\ 30,\ 60\ s$) and layer thicknesses adopted in the photopolymerization process: $h_i = 0.03\ mm$ (a), $h_i = 0.05\ mm$ (b), $h_i = 0.07\ mm$ (c).
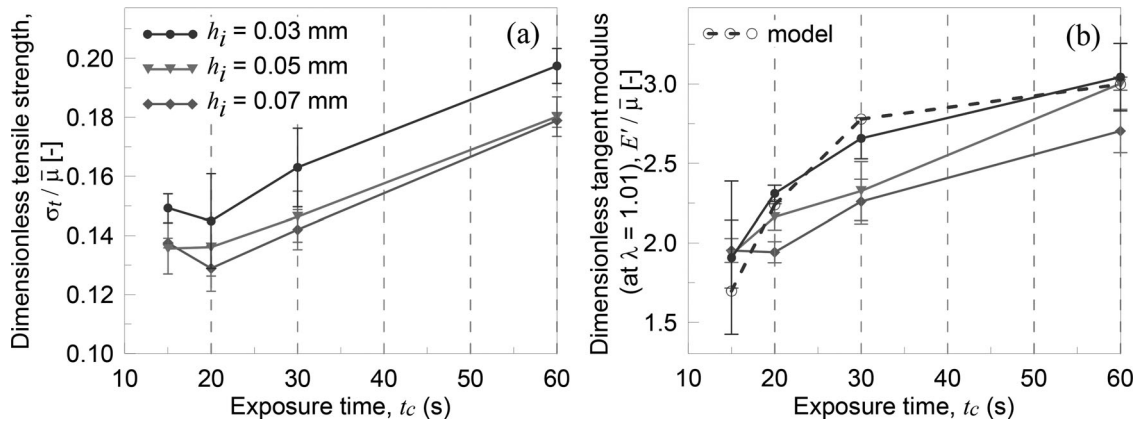

Figure 6. Photopolymer No. 2. Dimensionless mean tensile strength and dimensionless mean tangent Young's modulus (determined at the deformation $\lambda = 1.01$) vs exposure time for different layer thicknesses ($h_i = 0.03,\ 0.05,\ 0.07\ mm$).

related prediction is reported in Figure 4b. The curing time t_c results to have a crucial role on both the elastic constant and the tensile strength values; both of them noticeably increase upon longer times of exposure to the UV light. The tensile strength of the material turns out to be slightly dependent on the layer thickness when the maximum time exposure ($t_c = 60\ s$) is considered (Figure 4a). Lower exposure times ($t_c = 10 \div 30\ s$) provide a lower strength which results also to be more influenced by the layer thickness. Unexpectedly, the Young's modulus and the tensile strength for the layer thickness $h_i = 0.03\ mm$ result to be lower than those for $h_i = 0.05\ mm$ for $t_c = 20,\ 30\ s$, while this inversion does not

occur for $t_c = 10,\ 60\ s$; this could be related to the low thickness difference and to experimental uncertainties.

The results for the photopolymer No. 2 follow a trend similar to that of the photopolymer No. 1; as before, the exposure time plays the major role on the tensile strength (Figure 5a) as well as on the tangent elastic modulus (Figure 5b).

Figure 6a and b show that both the tensile strength and the tangent Young's modulus increase with the exposure time and slightly decrease by increasing the layer thickness; as expected, printing by adopting thinner layers ensures a greater elastic modulus and a higher tensile strength of the material.
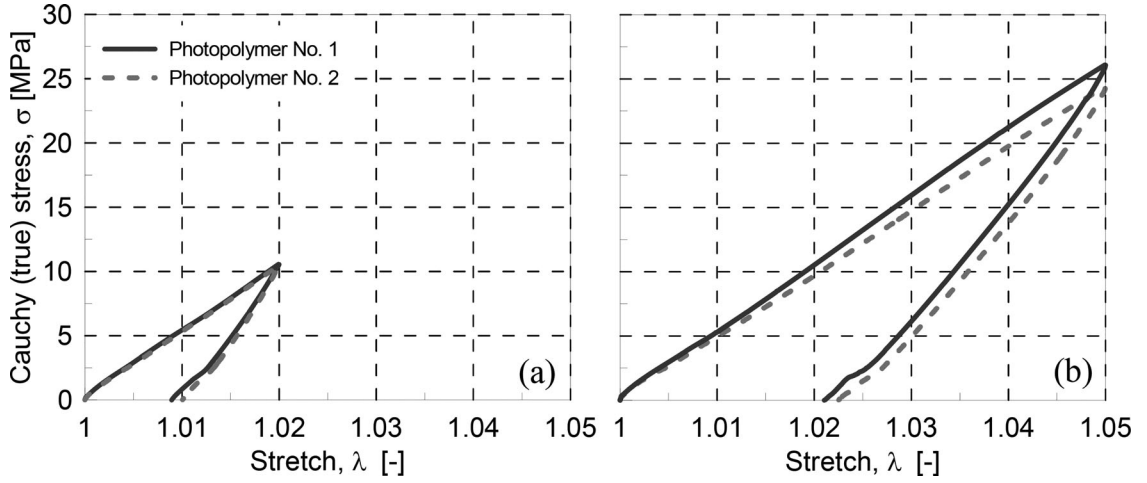
Figure 7. True stress vs stretch displayed by the photopolymers No. 1 and 2 ($t_c = 30s$) under a full stress cycle up to a maximum deformation equal to $\lambda = 1.02$ (a) and $\lambda = 1.05$ (b).

By considering the value of the elastic modulus of the photopolymer No. 2 obtained for a large value of the curing time, the asymptotic value of the shear modulus, corresponding to the fully cured condition, results to be equal to about $\overline{\mu} = 230\ MPa$. Figure 6 shows the mean values and the related standard deviations of the strength and of the Young's modulus for the photopolymer No. 2; as observed for the previous polymer, the curing time t_c plays the main role on both the elastic modulus and the tensile strength; both of them increase for longer time exposure to the UV light. The effectiveness of using thinner layers in the AM process on the considered mechanical properties is also clearly visible. The model prediction (parameters of the model: $k_p = k_t = 0.6\ \frac{m^3}{mol\ s}$, $\gamma = 8 \cdot 10^{-3} \frac{s^2}{kg}$, $\alpha = 3$, $C_I = 500 \frac{mol}{m^3}$, $C_{M0} = 3000 \frac{mol}{m^3}$, $C_R = 0 \frac{mol}{m^3}$, $A = 147\ m^{-1}$) is reported in Figure 6b; the dimensionless elastic modulus is in good agreement with the corresponding experimental values.

Finally, in order to verify if during the applied deformation the material displays damage, cyclic tests have been performed up to the stretch values $\lambda = 1.02,\ 1.05$; Figure 7 clearly demonstrates that material degradation occurs even for low values of the applied stretch. This aspect will be considered in Sect. 5 where a simple damage model will be introduced.

4. Micromechanical model

4.1. Micromechanical constitutive model of a polymer network

Polymeric materials, such as rubbers, gels, etc., are characterized by an amorphous microstructure made of a network of long entangled chains, coiled together and eventually reciprocally joined at discrete points termed as cross-links. The high level of disorder existing in a polymer network is well described by the entropic energy, which can be usefully associated to the network conformation state [33–35]. The classical freely-jointed chain model is usually adopted to describe the topology of network chains; each chain is assumed to be made of N rigid segments of equal length b, organized in the 3 D space according to the so-called random walk theory, while the chain's ends are at a distance

$r = (r_x, r_y, r_z)$ apart; this latter quantity is used to quantify the deformed state of the chain.

The description of the physical state of the polymer can be conveniently done by using the statistics of the end-to-end vector distribution; it is mathematically provided by the chain distribution function $\rho(r)$. For a given state of the material, it quantifies the number of network's chains with a given end-to-end vector r. The statistical distribution function can be expressed as $\rho(r,t) = c_a\ \varphi_0(r,t)$, where c_a is the chain concentration (number of mechanically active chains per unit volume), while $\varphi(r)$ is the dimensionless distribution function, often adopted to be the standard Gaussian with mean value $r = 0$ and standard deviation $b\sqrt{N/3}$ [35]. In the mechanics of polymers, the affine deformation hypothesis is usually adopted: it ensures that the length of a deformed chain is expressed as $r = |r| = \lambda |r_0|$ (being $r_0 = b\sqrt{N}$ the chain's mean square length in the network stress-free state), where λ is the macroscopic deformation of the material. The affine deformation hypothesis is adopted hereafter, i.e. the polymer chain's stretch is assumed to be that experienced by the material at the continuum scale, namely λ.

The energy density stored in the polymer network can be evaluated by summing up the deformation energy of the single chains, whose end-to-end distance distribution is provided by the distribution function $\rho(r)$, as follows [36]:

$$\Psi(t) = \int_{\Omega} \rho(r,t)\ \psi(r)\ d\Omega = c_a(t)\langle \varphi(r,t)\ \psi(r)\rangle \tag{5}$$

The energy per single chain ψ is usually set to depend on the chain's end-to-end distance only; by adopting the Langevin statistics, suitable for a wide range of chain deformations, the energy per single chain is expressed as [35]:

$$\psi = N\ k_B T \cdot \left(\beta \frac{\lambda}{\sqrt{N}} + \ln \frac{\beta}{\sinh\beta} \right), \quad \beta = \mathcal{L}^{-1}\left(\frac{r}{bN} \right)$$
$$= \mathcal{L}^{-1}\left(\frac{\lambda}{\sqrt{N}} \right) \tag{6}$$

where the inverse $\mathcal{L}^{-1}(\blacksquare)$ of the Langevin function $\mathcal{L}(\blacksquare)$, defined as: $\mathcal{L}(\blacksquare) = \coth(\blacksquare) - \blacksquare^{-1}$, has been introduced. Such an inverse function is well approximated by the
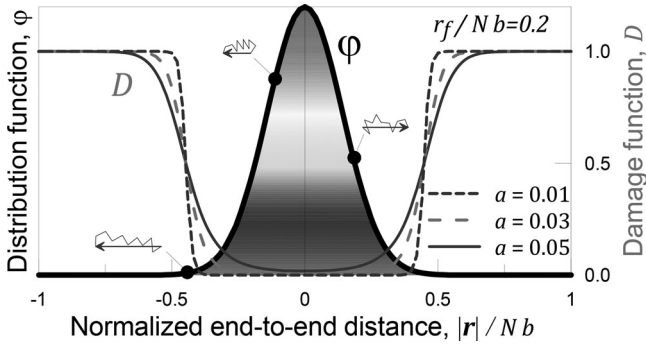
Figure 8. 1 D scheme of the dimensionless chain distribution function φ and of the damage function D quantifying the likelihood that a given stretched chain leaves the deformed network (three values of the parameter a are considered for the function D, see Eq. 11).

expression $\mathcal{L}^{-1}(x) = G(x) \cong x\frac{x^2-3x+3}{1-x}$ [37] which is particularly useful in the numerical analyses of real cases.

Further details on the mechanical governing equation of a polymer network whose response is governed mainly by entropic effects are provided in Appendix B.

If the material responds in an inelastic way, because some of its network chains are lost due to their breakage, the evolution in time of the distribution function $\rho(\boldsymbol{r})$ [38] can be generalized by accounting for such a damage mechanism. The time rate of the chain distribution function is expressed as [36]:

$$\dot{\rho}(\boldsymbol{r}) = \dot{\rho}_F(\boldsymbol{r}) + \dot{\rho}_V(\boldsymbol{r}) + \dot{\rho}_D(\boldsymbol{r}) =$$
$$= -[\boldsymbol{L} : \nabla \boldsymbol{F} \otimes \boldsymbol{r}] - [tr\boldsymbol{L} \ \rho(\boldsymbol{r})] - k \ [\rho(\boldsymbol{r}) - \rho_0(\boldsymbol{r})] \ D(|\boldsymbol{r}|) \tag{7}$$

where the term $\dot{\rho}_F$ accounts for the variation due to the deformation, $\dot{\rho}_V$ quantifies the rate produced by the volume variation (it is zero in an isochoric deformation, being $tr\boldsymbol{L} = 0$) and $\dot{\rho}_D$ quantifies the effect of internal damage (loss of chains). Physically, the last term represents chains detaching from the actual deformed network configuration ρ, at the rate k, and eventually enter into play again in the reference stress-free state (represented by the distribution ρ_0); according to this assumption, after failing, the chains are still able to bear a force, starting from the reference state, because of the entanglement existing with the surrounding chains. In Eq. (7) the damage parameter D has been introduced in order to consider the deformation-dependence of the chain failure mechanism. A suitable expression for D is provided by the following sigmoidal function

$$D(|\boldsymbol{r}|) = \frac{1}{1 + e^{-\frac{|\boldsymbol{r}|-r_f}{a}}} \tag{8}$$

where r_f represents the chain end-to-end distance beyond which the failure starts to occur and a is a model parameter. According to the structure of Eq. (7), this damage model also enables to take into account the strain rate effect, since the term $k \ [\rho - \rho_0] \ D$ quantifies the number of chains leaving the deformed network (ρ), and entering into the undeformed one (ρ_0), per unit time. According to this model, not enough stretched chains (low values of $|\boldsymbol{r}|$) do not detach from the network ($D \cong 0$), while chains having a

sufficiently high end-to-end distance are more likely to fail ($D \cong 1$ for $|\boldsymbol{r}| > r_f$), Figure 8.

4.2. Strength of a polymer network

The failure of a polymeric material corresponds to a progressive rupture of the network's chains; the initially active chains undergo failure when they reach a critical stretch which entails the overcoming of the bond strength existing among its atoms [39, 40]. Usually, the $C-C$ bond energy ($e_b = 5.767\text{E} - 19 \ J = 3.6 \ eV$, [40]) is adopted for estimating the energy required to induce scission in a single polymer chain. Once a single the $C-C$ bond breaks, the chain is no more able to contribute to the load bearing mechanism of the network and has to be neglected in the chain concentration, which accounts only for the active chains (i.e. those connected at both ends to the surrounding network), as defined above. The energy required to break all the chains contained in the unit volume, at least in one bond, is given by

$$\mathcal{E}_f = c_a \ e_b \tag{9}$$

On the other hand, when a polymer is stretched, its network stores the deformation energy density

$$\Delta\Psi(t) = \Psi(t) - \Psi_0 = c_a(t)\langle [\varphi(r,t) - \varphi_0(r)] \ \psi(r)\rangle \tag{10}$$

where $c_a(t) = $ const. if no chains are lost, while $c_a(t)$ is a non increasing function of time if damage takes place in the network. The network failure function $\mathcal{F}_n$ can thus be defined as:

$$\mathcal{F}_n(t) = \Delta\Psi(t) - c \ \mathcal{E}_f \begin{cases} \geq 0 \ \text{failure} \\ < 0 \ \text{no failure} \end{cases} \tag{11}$$

which states that the material breaks when the available deformation energy overcomes the energy required to separate at least one $C-C$ bond per chain. In the above expression, the material strength expressed in term of energy, $\mathcal{E}_f$, is multiplied by a chain scission energy reduction factor $c < 1$, required to account for all the micro defects and imperfections which reduce the energy $\mathcal{E}_f$ theoretically required to break all the chains contained in the unit volume of the material. In the next section, the present simple damage criterion is applied to estimate the tensile strength of the photopolymers experimentally studied in Section 3.

5. Numerical simulations

In this section, the micromechanical model is used to simulate the above-presented experimental tests. The mechanical properties of the two considered photopolymers have been assumed to be those provided by the photopolymerization model, Eqs (2)-(4), see Figures 4b and 6b. According to the values of the shear modulus of the two analyzed photopolymers in their fully cured state, namely $\overline{\mu} = 210 \ MPa$ and $\overline{\mu} = 230 \ MPa$ for the resin No.1 and No. 2, respectively, the corresponding chain concentrations in the mechanical model have been estimated to be equal to $\overline{c}_{a1} = c_{a1}(\varrho = 1) = 5.191 \ \cdot 10^{28}m^{-3}$ and $\overline{c}_{a2} = c_{a2}(\varrho = 1) = 5.686 \ \cdot 10^{28}m^{-3}$, while the deformation process has been always assumed to be isochoric, i.e. $\nu = 0.5$. Since the photopolymerization model presented in Section 2 does not
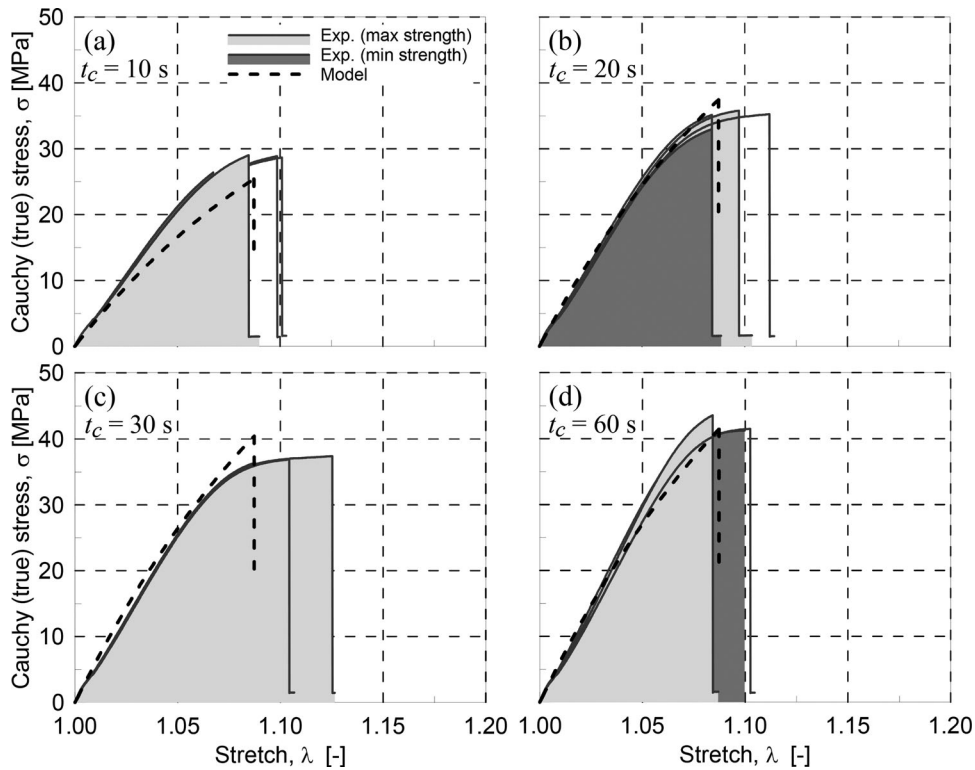
Figure 9. Experimental and model true stress vs stretch for the photopolymer No. 1 for different curing times: $t_c = 10s$ (a), $t_c = 20s$ (b), $t_c = 30s$ (c), and $t_c = 60s$ (d). The stress-deformation responses corresponding to the maximum and minimum strengths are filled in green and red color, respectively.

Figure 10. Experimental and model true stress vs stretch for the photopolymer No. 2 for different curing times: $t_c = 15s$ (a), $t_c = 20s$ (b), $t_c = 20s$ (c), and $t_c = 60s$ (d). The stress-deformation responses corresponding to the maximum and minimum strengths are filled in green and red color, respectively.
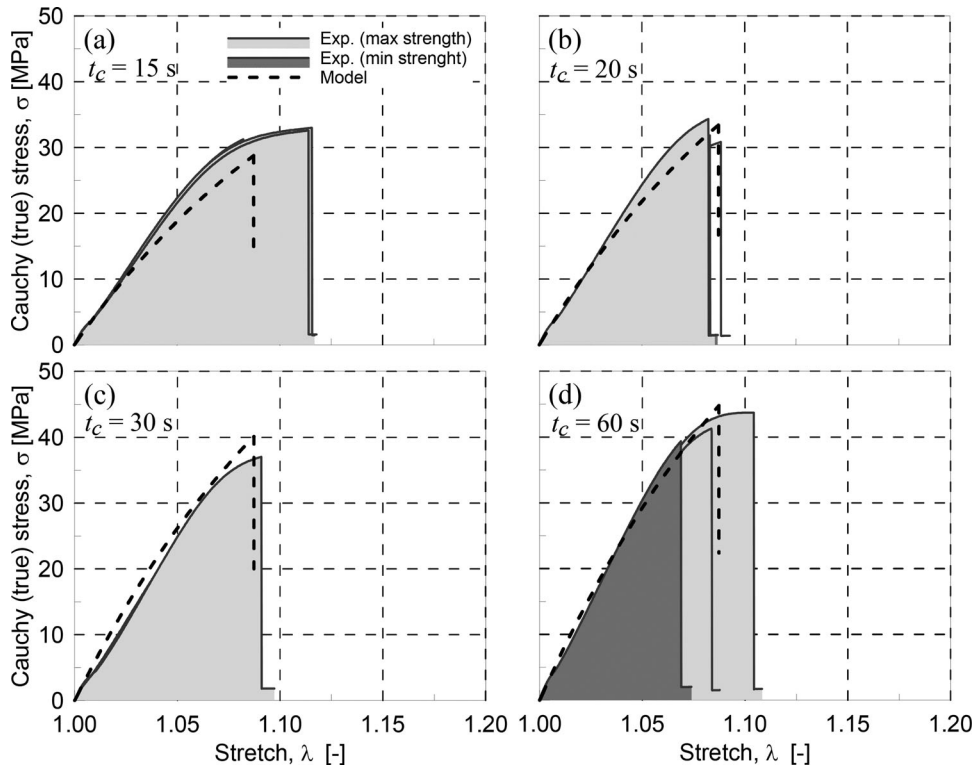
give noticeable differences in the mechanical properties of the photopolymerized material by changing the thickness of the layer being cured (see Figures 4b and 6b), such a parameter has been neglected and the average layer thickness value $h_i = 0.05\ mm$ has been adopted in the following.

The damage mechanism occurring at the network level, which is responsible for the material failure, has been modeled through the chains detachment and re-attachment model previously illustrated. The model parameters have been calibrated on the basis of the experimental tests; in all the simulations we
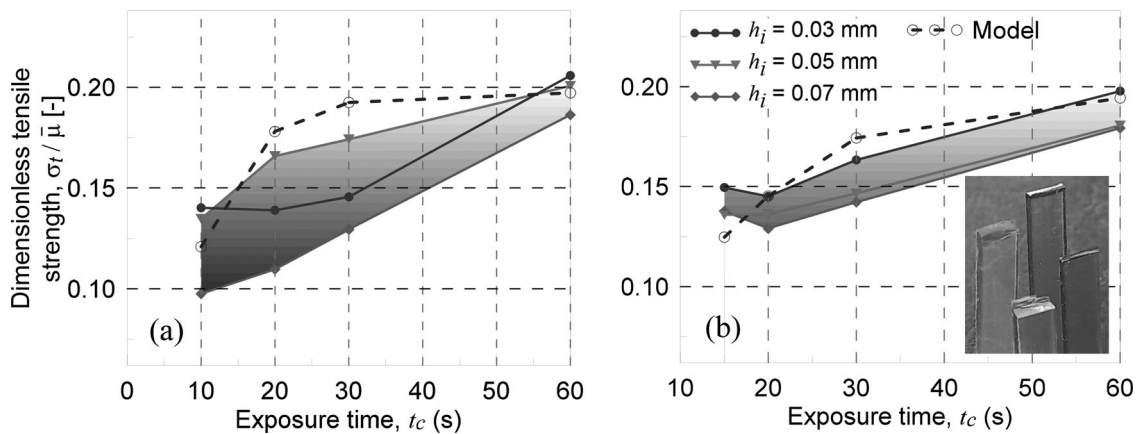
Figure 11. Comparison of the tensile strength vs exposure time provided by experimental results (interpolation curves of the experimental results are displayed) and by the theoretical model for the photoresins No. 1 (a) and No. 2 (b). Detail: appearance of the broken specimens.

adopt: $r_f/Nb = 0.7$, chain detachment rate $k = 0.4$, chain scission energy reduction factor $c = 1.4E - 4$.

Figure 9 illustrates the true stress *vs* stretch up to the final failure for the photopolymer No. 1 cured by using different light exposure times; model results are also reported for comparison. Similarly, Figure 10 illustrates the true stress *vs* stretch curves for the photopolymer No. 2. The $\sigma - \lambda$ curves provided by the model are represented as dashed lines up to the final predicted failure of the material whose tensile strength has been estimated on the basis of the failure criterion expressed by Eq. (11).

Finally, Figure 11 displays the experimental tensile strengths obtained for the photopolymers No. 1 and 2 for the various exposure times and those provided by the model. It is worth mentioning that the assessment of the failure strength of brittle polymers, as those here considered, is not simple and is affected by various uncertainties related to the applied strain rate, the material imperfections, etc. However, despite the simplicity of the proposed model, the tensile strength is properly estimated by the model, even if a certain overestimation of the strength can be appreciated for intermediate values of the curing time t_c.

It is worth noting that the present study has been performed by neglecting the effect of temperature on the kinetic of radical polymerization since all the experimental tests and numerical simulations have been conducted in isothermal conditions. Further, the strain rate effect that, in general, plays a role on the response of polymers, has not been accounted for; however, we restricted the analysis to small constant strain rate in order not to have such a dependence. Further, the statistical-based micromechanical model adopted for chain networks is based on the assumption that the material is governed by entropic effects only; this is not valid for highly stretched networks where standard enthalpic deformation energy must be also accounted for. Since in the present study the mechanical response has been explored limited to relatively small strains (up to 5%), the above-mentioned limitation are not so relevant here.

6. Conclusions

In the present study, the influence of the process parameters on the mechanical properties of photopolymerized polymers obtained through the radical polymerization has been considered from the experimental and theoretical perspectives. The radical polymerization (solidification), used in the so-called digital light processing (DLP) additive manufacturing (AM) technology, offers new potentialities for obtaining high precision parts spanning a wide dimensional scale range. Being the material's characteristics highly dependent on the way the process is conducted, this technology offers new design space freedom that can be exploited to precisely tune the mechanical properties of the printed material.

Here, we have considered the exposure time and the layer thickness as the main tunable parameters to be used as design variables for controlling the characteristics of the final material. It has been shown that the exposure time represents the main parameter affecting the mechanics of AM photopolymers, while the layer thickness – whose influence is strictly related to the transparency of the material – resulted to be less important because of the high transparency of the liquid resin as well as of the solid polymer analyzed here. We have proposed a multi-physics approach based on the light diffusion, the photopolymerization chemical kinetics and a statistical-based micromechanics model to assess the resulting mechanical properties of the material. The multi-physics simulation tool, requiring few physics-based parameters easily tunable in real cases, has provided reasonable results in terms of elastic modulus, tensile strength and stress-deformation response for this class of photopolymers.

The proposed multi-chemical-physics model, being based on a detailed description of the main involved chemical-physics phenomena, allows us to precisely control the AM process in order to obtain the desired mechanical properties of the printed part starting from the initial liquid monomer. Once all the concentrations of the initial liquid resin are known, one can play with all the printing parameters (exposure time, light intensity and distribution, layer thickness, absorbance of the material in function of its degree of solidification, etc.) to reach the desired material's characteristics. From this perspective, photopolymerization offers a huge design space allowing to control and develop new materials characterized by specific properties.

Because of the raising interest in AM processes and their extensive use for the production of load bearing parts, the precise knowledge of the way the involved parameters affect the properties of the obtained material is nowadays required as a matter of urgency; in this context, the proposed physics-based theoretical approach has the potentialities to be used as a design tool to define how the photopolymerization process has to be performed with respect to the desired characteristics of the final material.

Disclosure statement

No potential conflict of interest was reported by the authors.

Authors contributions

RB conceived the research, designed and performed the numerical analyses and wrote the paper; MPM and MM prepared the samples and performed the experimental tests; LM and MPC participated in the revision of the manuscript. All authors read and approved the final manuscript.

Funding

Data availability

Data related to the present research are available upon request to the authors.

References

[1] K. V. Wong, and A. Hernandez, A review of additive manufacturing, ISRN Mech. Engin., vol. 2012, pp. 1–10, 2012. DOI: 10.5402/2012/208760.

[2] H. Bikas, P. Stavropoulos, and G. Chryssolouris, Additive manufacturing methods and modelling approaches: a critical review, Int. J. Adv. Manuf. Technol., vol. 83, no. 1–4, pp. 389–405, 2016. DOI: 10.1007/s00170-015-7576-2.

[3] R. Brighenti, M. P. Cosma, L. Marsavina, et al., Laser-based additively manufactured polymers: a review on processes and mechanical models, J. Mater. Sci., vol. 56, no. 2, pp. 961–998, 2021. DOI: 10.1007/s10853-020-05254-6.

[4] A. Iqbal, G. Zhao, H. Suhaimi, N. He, G. Hussain, and W. Zhao, Readiness of subtractive and additive manufacturing and their sustainable amalgamation from the perspective of Industry 4.0: a comprehensive review, Int. J. Adv. Manuf. Technol., vol. 111, no. 9–10, pp. 2475–2498, 2020. DOI: 10.1007/s00170-020-06287-6.

[5] M. Javaid, A. Haleem, R. P. Singh, R. Suman, and S. Rab, Role of Additive Manufacturing applications towards environmental sustainability, Adv. Ind. Eng. Polym. Res., vol. 4, no. 4, pp. 312–322, 2021. DOI: 10.1016/j.aiepr.2021.07.005.

[6] R. Leal, et al., Additive manufacturing tooling for the automotive industry, Int. J. Adv. Manuf. Technol., vol. 92, no. 5–8, pp. 1671–1676, 2017. DOI: 10.1007/s00170-017-0239-8.

[7] A. A. Shapiro, et al., Additive manufacturing for aerospace flight applications, J Spacecraft and Rockets., vol. 53, no. 5, pp. 952–959, 2016. DOI: 10.2514/1.A33544.

[8] B. Lu, H. Lan, and H. Liu, Additive manufacturing frontier: 3D printing electronics, Opto-Electr Adv., vol. 1, no. 1, pp. 17000401–17170004, 2018. DOI: 10.29026/oea.2018.170004.

[9] N. Singh, and G. Singh, Advances in polymers for bio-additive manufacturing: A state of art review, J. Manuf. Processes., vol. 72, pp. 439–457, 2021. DOI: 10.1016/j.jmapro.2021.10.045.

[10] D. Han, Y. Wang, C. Yang, and H. Lee, Multimaterial printing for cephalopod-inspired light-responsive artificial chromatophores, ACS Appl. Mater. Interfaces., vol. 13, no. 11, pp. 12735–12745, 2021. DOI: 10.1021/acsami.0c17623.

[11] M. Al Khalil, N. Lebaal, F. Demoly, and S. Roth, A design and optimization framework of variable-density lattice structures for additive manufacturing, Mech. Adv. Mater. Struct., pp. 1–15, 2021. DOI: 10.1080/15376494.2021.1936704.

[12] W. Y. Yeong, and G. D. Goh, 3D printing of carbon fiber composite: the future of composite industry?, Matter., vol. 2, no. 6, pp. 1361–1363, 2020. DOI: 10.1016/j.matt.2020.05.010.

[13] S. Roh, D. P. Parekh, B. Bharti, S. D. Stoyanov, and O. D. Velev, 3D printing by multiphase silicone/water capillary inks, Adv. Mater., vol. 29, no. 30, pp. 1701554, 2017. DOI: 10.1002/adma.201701554.

[14] D. Han, Z. Lu, S. A. Chester, and H. Lee, Micro 3D printing of a temperature-responsive hydrogel using projection microstereolithography, Sci. Rep., vol. 8, no. 1, pp. 1–10, 2018. DOI: 10.1038/s41598-018-20385-2.

[15] P. J. Bártolo, Stereolithographic processes. In: Stereolithography, Springer, Boston, MA, pp. 1–36, 2011. ISBN: 978-0-387-92904-0

[16] H. W. Kang, J. H. Park, and D. W. Cho, A pixel based solidification model for projection based stereolithography technology, Sens. Actuators, A., vol. 178, pp. 223–229, 2012. DOI: 10.1016/j.sna.2012.01.016.

[17] J. R. Tumbleston, et al., Additive manufacturing. Continuous liquid interface production of 3D objects, Science., vol. 347, no. 6228, pp. 1349–1352, 2015. DOI: 10.1126/science.aaa2397.

[18] K. L. Sampson, et al., Multimaterial vat polymerization additive manufacturing, ACS Appl. Polym. Mater., vol. 3, no. 9, pp. 4304–4324, 2021. DOI: 10.1021/acsapm.1c00262.

[19] K. Chockalingam, N. Jawahar, K. N. Ramanathan, and P. S. Banerjee, Optimization of stereolithography process parameters for part strength using design of experiments, Int. J. Adv. Manuf. Technol., vol. 29, no. 1–2, pp. 79–88, 2006. DOI: 10.1007/s00170-004-2307-0.

[20] S. A. Tofail, E. P. Koumoulos, A. Bandyopadhyay, S. Bose, L. O'Donoghue, and C. Charitidis, Additive manufacturing: scientific and technological challenges, market uptake and opportunities, Mater. Today., vol. 21, no. 1, pp. 22–37, 2018. DOI: 10.1016/j.mattod.2017.07.001.

[21] M. F. Perry, and G. W. Young, A mathematical model for photopolymerization from a stationary laser light source, Macromol. Theory Simul., vol. 14, no. 1, pp. 26–39, 2005. DOI: 10.1002/mats.200400056.

[22] R. Brighenti, M. P. Cosma, L. Marsavina, A. Spagnoli, and M. Terzano, Multiphysics modelling of the mechanical properties in polymers obtained via photo-induced polymerization, Int. J. Adv. Manuf. Technol., vol. 117, no. 1–2, pp. 481–499, 2021. DOI: 10.1007/s00170-021-07273-2.

[23] K. Classens, T. Hafkamp, S. Westbeek, J. J. Remmers, and S. Weiland, Multiphysical modeling and optimal control of material properties for photopolymerization processes, Addit. Manuf., vol. 38, pp. 101520, 2021. DOI: 10.1016/j.addma.2020.101520.

[24] J. Wu, Z. Zhao, C. M. Hamel, et al., Evolution of material properties during free radical photopolymerization, J. Mech. Phys. Solids., vol. 112, pp. 25–49, 2018. DOI: 10.1016/j.jmps.2017.11.018.

[25] S. F. Edwards, The theory of rubber elasticity, Brit. Poly. J., vol. 9, no. 2, pp. 140–143, 1977. DOI: 10.1002/pi.4980090209.

[26] R. Brighenti, and M. P. Cosma, Mechanical behavior of photopolymerized materials, J. Mech. Phys. Solids., vol. 153, pp. 104456, 2021. DOI: 10.1016/j.jmps.2021.104456.

[27] C. N. Bowman, and C. J. Kloxin, Toward an enhanced understanding and implementation of photopolymerization reactions, AIChE J., vol. 54, no. 11, pp. 2775–2795, 2008. DOI: 10.1002/aic.11678.

[28] A. Lubatsch, J. Kroha, and K. Busch, Theory of light diffusion in disordered media with linear absorption or gain, Phys. Rev. B., vol. 71, no. 18, pp. 184201, 2005. DOI: 10.1103/PhysRevB.71.184201.

[29] A. Bagheri, K. E. Engel, C. W. A. Bainbridge, J. Xu, C. Boyer, and J. Jin, 3D printing of polymeric materials based on photo-RAFT polymerization, Polym. Chem., vol. 11, no. 3, pp. 641–647, 2020. DOI: 10.1039/C9PY01419E.

[30] A. Bagheri, C. M. Fellows, and C. Boyer, Reversible deactivation radical polymerization: From polymer network synthesis to 3D printing, Adv. Sci. (Weinh)., vol. 8, no. 5, pp. 2003701, 2021. DOI: 10.1002/advs.202003701.

[31] M. Zarrelli, A. A. Skordos, and I. K. Partridge, Toward a constitutive model for cure-dependent modulus of a high temperature epoxy during the cure, Eur. Polym. J., vol. 46, no. 8, pp. 1705–1712, 2010. DOI: 10.1016/j.eurpolymj.2010.06.002.

[32] ISO 527-1. Plastics — Determination of Tensile Properties — Part 1: General Principles, ISO (International Organization for Standardization), Switzerland, 2019.

[33] P. J. Flory, and J. Rehner, Statistical mechanics of cross-linked polymer networks. I. Rubberlike elasticity, J. Chem. Phys., vol. 11, no. 11, pp. 512–520, 1943. DOI: 10.1063/1.1723791.

[34] L. R. G. Treloar, The Physics of Rubber Elasticity, L. R. G. Treloar, 3rd ed. Clarendon Oxford, Oxford, UK, 1975. DOI: 10.1002/pi.4980080107.

[35] M. Doi, Introduction to Polymer Physics. Oxford University Press, Oxford, UK, 1996. ISBN-10: 0198517890

[36] F. J. Vernerey, R. Long, and R. Brighenti, A statistically-based continuum theory for polymers with transient networks, J. Mech. Phys. Solids., vol. 107, pp. 1–20, 2017. DOI: 10.1016/j.jmps.2017.05.016.

[37] E. Darabi, and M. Itskov, A generalized tube model of rubber elasticity, Soft Matter., vol. 17, no. 6, pp. 1675–1684, 2021. DOI: 10.1039/D0SM02055A.

[38] F. J. Vernerey, R. Brighenti, R. Long, and T. Shen, Statistical damage mechanics of polymer networks, Macromolecules., vol. 51, no. 17, pp. 6609–6622, 2018. DOI: 10.1021/acs.macromol.8b01052.

[39] Y. Mao, and L. Anand, Fracture of elastomeric materials by crosslink failure, J. Appl. Mech., vol. 85, no. 8, 2018. DOI: 10.1115/1.4040100.

[40] Y. Mao, B. Talamini, and L. Anand, Rupture of polymers by chain scission, Extreme Mech. Lett., vol. 13, pp. 17–24, 2017. DOI: 10.1016/j.eml.2017.01.003.

[41] J. T. Lin, H. W. Liu, K. T. Chen, and D. C. Cheng, Modeling the kinetics, curing depth, and efficacy of radical-mediated Photopolymerization: the role of oxygen inhibition, viscosity, and dynamic light intensity, Front. Chem., vol. 7, pp. 760, 2019. DOI: 10.3389/fchem.2019.00760.

[42] Y. Yang, L. Li, and J. Zhao, Mechanical property modeling of photosensitive liquid resin in stereolithography additive manufacturing: bridging degree of cure with tensile strength and hardness, Mater. Design., vol. 162, pp. 418–428, 2019. DOI: 10.1016/j.matdes.2018.12.009.

Appendix A

Kinetics of chemical species evolution

The kinetics of the concentration evolution of the involved species is quantified by the following differential equations:

$$Ph_I \xrightarrow{\gamma} 2R^\bullet \quad \dot{C}_I(\boldsymbol{X},t) = -\gamma\, I(\boldsymbol{X},t)\, C_I(\boldsymbol{X},t) \tag{A1}$$

$$R^\bullet + M \xrightarrow{k_p} P^\bullet \ \text{and} \ P^\bullet + M \xrightarrow{k_p} P^\bullet$$
$$\dot{C}_R(\boldsymbol{X},t) = -m\,\dot{C}_I(\boldsymbol{X},t) - m\, k_t(\boldsymbol{X},t)[C_R(\boldsymbol{X},t)]^2 \tag{A2}$$

$$P^\bullet + R^\bullet \xrightarrow{k_t} P_{dead} \ \text{and} \ P^\bullet + P^\bullet \xrightarrow{k_t} P_{dead}$$
$$\dot{C}_M(\boldsymbol{X},t) = -k_p(\boldsymbol{X},t) C_M(\boldsymbol{X},t) C_R(\boldsymbol{X},t) \tag{A3}$$

$$\dot{\varrho}(\boldsymbol{X},t) = \frac{k_p(\boldsymbol{X},t) C_M(\boldsymbol{X},t) C_R(\boldsymbol{X},t)}{C_{M0}} \tag{A4}$$

where $\dot{\blacksquare}$ indicates the time derivative of the generic quantity, $\dot{\blacksquare} = \frac{\partial\blacksquare}{\partial t}$, γ is the photodecomposition rate, m is the number of radicals generated in the photodecomposition (typically $m = 2$), k_t is the termination rate ($k_t(t) = k_{t0} \cdot g(\varrho)$, being k_{t0} its initial value and g a cure-dependent parameter related to the diffusion-controlled termination), and k_p is the propagation rate constant (also function of the curing evolution). To complete the picture of the involved reactions, it is worth recalling that the chain formation is hindered by the presence of other chemical species, such as oxygen, which can slow down and reduce the effectiveness of the polymer chain formation [24, 29–31, 41, 42].

According to Eq. (2) and Eq. (A1), the time rate of the degree of cure is given by: $\dot{\varrho}(\boldsymbol{X},t) = k_p(\boldsymbol{X},t)\frac{C_M(\boldsymbol{X},t)C_R(\boldsymbol{X},t)}{C_{M0}}$, so the actual degree of cure can be estimated, once the initial values of the involved quantities, $C_I(\boldsymbol{X}, t=0)$, $C_R(\boldsymbol{X}, t=0)$, $C_M(\boldsymbol{X}, t=0)$, as well as $I(\boldsymbol{X},t)$ are known, through the integration of the above quantity over the time interval $(0, \ t)$.

Appendix B

Micromechanical constitutive model of a chain network

The tensile force acting on a chain (always directed as the vector $\boldsymbol{r}$) is provided by the derivative of ψ with respect to the vector $\boldsymbol{r}$, i.e. $\boldsymbol{f} = \frac{\partial\psi}{\partial\boldsymbol{r}} = \frac{\boldsymbol{r}}{|\boldsymbol{r}|} \cdot \frac{k_B T}{b} \cdot \mathcal{L}^{-1}\left(\frac{\lambda}{\sqrt{N}}\right)$, being λ the macroscopic deformation. Alternatively, a simpler expression valid when the Gaussian statistics is assumed, provides the energy per chain to be $\psi = \frac{3k_B T}{2Nb^2}|\boldsymbol{r}|^2$, while in this case $\boldsymbol{f} = -\frac{3k_B T}{Nb^2}|\boldsymbol{r}| = \frac{3k_B T}{b\sqrt{N}}\lambda$. Upon derivation of the free energy density with respect to the deformation gradient, the 1st Piola stress tensor $\boldsymbol{P}$ can be determined and the true (Cauchy) stress tensor can be finally obtained accordingly:

$$\begin{aligned}
\boldsymbol{\sigma} &= J^{-1} \underbrace{\boldsymbol{P}}_{\frac{\partial\boldsymbol{\Psi}}{\partial\boldsymbol{F}}} \boldsymbol{F}^T = c_a \int_\Omega \left[\varphi(\boldsymbol{r},t) - \varphi_0(\boldsymbol{r})\right] \frac{\partial\psi}{\partial\boldsymbol{r}} \otimes \boldsymbol{r}\ d\boldsymbol{\Omega} + p\mathbf{1} \\
&= \left\langle c_a\left[\varphi(\boldsymbol{r},t) - \varphi_0(\boldsymbol{r})\right]\boldsymbol{f} \otimes \boldsymbol{r}\right\rangle + p\mathbf{1} \\
&= \frac{k_B T}{b}\mathcal{L}^{-1}\left(\frac{\lambda}{\sqrt{N}}\right)\left\langle c_a\left[\varphi(\boldsymbol{r},t) - \varphi_0(\boldsymbol{r})\right]\frac{1}{|\boldsymbol{r}|}\boldsymbol{r} \otimes \boldsymbol{r}\right\rangle
\end{aligned} \tag{B1}$$

where we have indicated with $\langle\blacksquare\rangle = \int_\Omega \blacksquare d\Omega = \int_0^{2\pi}\int_0^\pi\left(\int_0^{Nb}\blacksquare\ r^2 dr\right)\sin\theta d\theta d\beta$, the integration over the chain configuration space, being θ, β the Euler angles of the end-to-end vector $\boldsymbol{r}$ in the 3 D space. In Eq. (B1) p is the hydrostatic stress introduced for enforcing the isochoric deformation, corresponding to $J = \det\boldsymbol{F} = 1$, assumed to be true for the material under study. The fourth-order elasticity tensor is finally given by:

$$\begin{aligned}
\boldsymbol{C} &= \frac{\partial\boldsymbol{\sigma}}{\partial\boldsymbol{F}} = c_a\frac{k_B T}{b}\frac{\partial}{\partial\boldsymbol{F}}\left[\mathcal{L}^{-1}\left(\frac{\lambda}{\sqrt{N}}\right)\left\langle\varphi(\boldsymbol{r},t)\frac{1}{|\boldsymbol{r}|}\boldsymbol{r}\otimes\boldsymbol{r}\right\rangle\right] \\
&= c_a\frac{k_B T}{b}\left\{\boldsymbol{G}'\left\langle\varphi(\boldsymbol{r},t)\frac{1}{|\boldsymbol{r}|}\boldsymbol{r}\otimes\boldsymbol{r}\right\rangle + \frac{1}{|\boldsymbol{r}|}\mathcal{L}^{-1}\left(\frac{\lambda}{\sqrt{N}}\right)\left\langle[-\boldsymbol{F}^{-1}\nabla\boldsymbol{\varphi}\otimes\boldsymbol{r}]^T\boldsymbol{r}\otimes\boldsymbol{r}\right\rangle\right\} \\
&= c_a\frac{k_B T}{b}\left\{b\sqrt{N/3}\ \boldsymbol{G}'\otimes\mathbf{1} + \frac{G}{|\boldsymbol{r}|}\left\langle[-\boldsymbol{F}^{-1}\nabla\varphi\otimes\boldsymbol{r}]^T\otimes(\boldsymbol{r}\otimes\boldsymbol{r})\right\rangle\right\}
\end{aligned} \tag{B2}$$

where in a one dimensional case ($F_{11} = \lambda$, $F_{ii} = 1$, $i = 2,3$, $F_{ij} = 0$, $i \neq j$), $G'_{11} = \frac{\partial}{\partial\lambda}\left(\xi\frac{\xi^2 - 3\xi + 3}{1 - \xi}\right) = -\frac{1}{\sqrt{N}}\frac{2\xi^2 - 6\xi^2 + 6\xi - 3}{(\xi - 1)^2}$, having set $\xi = \frac{\lambda}{\sqrt{N}}$.